SpezialForschungsBereich F 32

Karl–Franzens Universität Graz
Technische Universität Graz
Medizinische Universität Graz

Nonlinear Inversion in Fluorescence Optical Tomography

M.Freiberger H. Egger H. Scharfetter

SFB-Report No. 2009–078 Dezember 2009

A–8010 GRAZ, HEINRICHSTRASSE 36, AUSTRIA

Supported by the
Austrian Science Fund (FWF)

SFB sponsors:

- **Austrian Science Fund** (FWF)
- **University of Graz**
- **Graz University of Technology**
- **Medical University of Graz**
- **Government of Styria**
- **City of Graz**

Nonlinear Inversion in Fluorescence Optical Tomography

Manuel Freiberger *Student Member, IEEE*, Herbert Egger, and Hermann Scharfetter

***Abstract*—Fluorescence optical tomography is a non-invasive imaging modality that employs the absorption and re-emission of light by fluorescent dyes. The aim is to reconstruct the fluorophore distribution in a body from measurements of light intensities at the boundary. Due to the diffusive nature of light propagation in tissue, fluorescence tomography is a nonlinear and ill-posed inverse problem, and some sort of regularzation is required for a stable solution. In this paper we investigate Tikhonov-type methods, and we utilize nonlinear penalty terms, namely total-variation regularization and a method of levelset type, which provide better reconstructions than standard L^2-penalty terms in cases where the unknown distributions are localized. We also propose iterative methods for the solution of the corresponding nonlinear least-squares problems, and discuss some details of a discretization by finite element methods, like the efficient assembly of the sensitivity system via adjoint methods. The improvement of reconstructions that can be obtained by utilizing nonlinear regularization terms is demonstrated in numerical examples.**

I. Introduction

Fluorescence diffuse optical tomography (FDOT) is a rather new imaging technology amongst the diffusion limited optical modalities. This method employs the ability of fluorescent dyes to absorb light in a certain wavelength range and to re-emit photons at a longer wavelength. The investigated sample, which can be a slice of tissue or a small animal, for example, is excited through a set of light sources placed on the surface of the sample. The excitation light then spreads through the tissue and is partially absorbed by fluorophores, which re-emit part of the light at a longer wavelength. The emitted light then spreads through the tissue again, and a part is recorded by detectores at the boundary.

A particularly advantageous feature of fluorescence tomography is the fact that the activity of fluorophores can be influenced by metabolical states or processes, like the oxygenation of the tissue [1], [2], the pH value [3], [4], or the temperature [5]. This enables *functional imaging*, i.e., to not only acquire anatomical images, but also to determine physiological activities in biological systems.

Three different measurement principles, which differ in the type of the excitation source, are mainly used nowadays: (i) continuous wave (CW) excitation with constant intensity [6], (ii) CW light with modulated intensity leading to frequency domain methods [7], [8], and (iii) time of flight-arrangements using ultra-short pulsed laser sources [9]. In this paper, we focus on the first two approaches.

Like other diffusion limited modalities, the spatial resolution of fluorescence optical tomography is rather low. The reason for this is that photons are scattered many times while traversing through the tissue, and thus their trajectories can be described only in a statistical manner. This leads to the ill-posedness of the inverse problem, i.e. the diffusive nature of light does not allow to reconstruct spatial details or high frequency components of the fluorophore concentration in a reliable way. In order to achieve a stable inversion, one has to use regularization methods and add a-priori information during the reconstruction. This can be assumptions about the distribution of the fluorescent dye or the covariance of the measurement data, see e.g. [10].

In order to simplify the light propagation models and to reduce the complexity of the inverse problem, Born approximations or similar linearizations of the forward system are frequently used in literature [11], [12]. Methods with linear regularization terms like the L^2- or H^1-norm are then applied for stable solution of the inverse problem, see e.g. [13].

In contrast to these approaches, we consider in this paper the full non-linear formulation of the forward problem, which is presented in section II-A. Additionally, we investigate the use of two non-linear regularization strategies: First, total-variation (TV) regularization, which penalizes variations in the fluorophore concentration, and second, a method of levelset type, which favours reconstructions with only two levels of fluorphore concentration; typically one level is assigned to the background, and another one to some object like a tumour or an organ. These two nonlinear methods are introduced in detail in section II-B. For the solution of the resulting nonlinear least-squares problems, we present in section III an efficient numerical algorithm based on Newton-type methods, and we report on numerical results obtained with the nonlinear regularization methods for simulated data in section IV.

II. Theoretical background

A. The forward model

For a mathematical description of the propagation of intensity modulated light in a turbid medium occupying the domain Ω, we utilize the following model [13]

$$-\nabla\cdot(\kappa_x\nabla\varphi_x)+\mu_x\varphi_x=q, \qquad \text{in } \Omega, \qquad (1)$$

$$-\nabla\cdot(\kappa_x\nabla\varphi_m)+\mu_m\varphi_m=\gamma c\varphi_x, \qquad \text{in } \Omega, \qquad (2)$$

This work has been submitted to the IEEE for possible publication. Copyright may be transferred without notice, after which this version may no longer be accessible. Financial support by the Austrian Science foundation (FWF) through grant F3207-N18 and SFB / F32 is gratefully ackowledged.

M. Freiberger and H. Scharfetter are with the Institute of Medical Engineering, Graz University of Technology, Kronesgasse 5/II, 8010 Graz, Austria. e-mail: {manuel.freiberger,hermann.scharfetter}@tugraz.at

H. Egger is with the Institute for Numerical Mathematics, Graz University of Technology, Steyrergasse 30, 8010 Graz, Austria. e-mail: herbert.egger@tugraz.at

where φ_i, $i = x, m$ denotes the complex amplitudes of the excitation (x) and emitted (m) light. If the dependence on the light source q is important, we write $\varphi_i(q)$. The functions κ_i, μ_i denote the photon diffusion and (complex) absorption coefficients at wavelengths λ_i. These parameters are related to more basic optical parameters and the fluorophore distribution by the following relations

$$\kappa_i = \frac{1}{3\left(\mu_{a,x} + \mu'_{s,x} + c\epsilon_x\right)}, \qquad (3)$$
$$\mu_i = \mu_{a,x} + c\epsilon_x + \frac{i\omega}{\nu}, \qquad \gamma = \frac{\eta}{1 - i\omega\tau}\epsilon_x.$$

Here, $\mu_{a,i}$, $\mu'_{s,i}$ are the absorption and reduced scattering coefficients characterizing the tissue under investigation; ϵ_i is the specific extinction coefficient of the fluorophore, i.e., $\mu_{f,i} = c\epsilon_i$ represents the additional absorption due to presence of the fluorophore; finally, η and τ denote the quantum efficiency and lifetime of the fluorescent marker, and ω and ν are the modulation frequency and the speed of light. For details on mathematical models for light propagation in fluorescence tomography, refer to [14], [15], and the references therein.

The system (1)–(3) is completed by Robin boundary conditions of the form

$$\rho_i\varphi_i + \kappa_i\partial_n\varphi_i = 0, \qquad \text{on } \partial\Omega, \qquad (4)$$

which model the assumption that no light can enter the domain Ω from outside. The parameters ρ_i allow to take into account a mismatch between the refractive indices of the tissue and the sourrounding space; see [16] for details and further references.

The measureable quantity in fluorescence tomography is the phase and intensity of the emitted light leaving the domain Ω, which is given by

$$\kappa_m\partial_n\varphi_m = -\rho_m\varphi_m. \qquad (5)$$

Assuming that a detector integrates the outgoing light over some area Δ_i of the boundary, the measurements at the i-th detector Δ_i resulting from the j-th excitation q_j can be defined as

$$M_{ij} = C_m \int_{\Delta_i} \varphi_m(q_j)\, ds, \qquad (6)$$

where C_m is a factor taking into account the characteristics of the detector and the reflection coefficient ρ_m. The measurement process that assigns to a given fluorophore distribution c and sources q_j, $j = 1, \dots, s$ the corresponding measurements M_{ij} at the detectors Δ_i, $i = 1, \dots, d$ can be described in compact form via the action of a *forward operator*

$$F : C_{ad} \subset L^2(\Omega) \to \mathbb{C}^{d\times s}, \quad c \mapsto M := [M_{ij}]_{i\le d, j\le s}. \qquad (7)$$

In order to guarantee solvability of the system (1)–(4), the set C_{ad} of admissible fluorophore distributions is defined as

$$C_{ad} := \{c \in L^2(\Omega) : 0 \le c \le \overline{c} \quad \text{in } \Omega\}, \qquad (8)$$

for some $\overline{c} > 0$. The forward problem of fluorescence tomography then consists of the determination of the measurement matrix $M = [M_{ij}]$ corresponding to a given fluorophore distribution c; this is achieved by solving the boundary value problems (1)–(4), and computing the measurements according to (6).

B. Inverse problem and regularization

The inverse problem of fluorescence tomography is the reconstruction of an unknown fluorophore distribution c from measurements M_{ij} of the emitted light φ_m for different detector locations Δ_i and sources q_j. In abstract form this reads

Inverse problem 1. *Given measurements M^δ of the emitted light φ_m for different detectors Δ_i, $i = 1, \dots, d$ and multiple excitations q_j, $j = 1, \dots, s$, find a fluorophore distribution $c \in C_{ad}$ such that*

$$F(c) = M^\delta, \qquad \|M^\delta - M\| \le \delta. \qquad (9)$$

Here, M^δ is some possibly perturbed approximation of the true data $M = [M_{ij}]_{ij}$ corresponding to the true fluorophore distribution c_f, and the noise level δ is a measure for the perturbations in the data.

For the stable solution of the inverse problem, we consider Tikhonov-type regularization methods, where the approximate solution $c^\delta_\alpha \in C_{ad}$ of (9) is defined as a minimizer of the regularized least-squares functional

$$J^\delta_\alpha(c) := \tfrac{1}{2}\|F(c) - M^\delta\|^2 + \alpha\mathcal{R}(c). \qquad (10)$$

The least-squares term penalizes the data misfit, while the regularization term $\mathcal{R}(c)$ has a stabilizing effect. The parameter $\alpha > 0$ allows to balance between approximation of the data and stability of the inversion. Assuming that $\mathcal{R}$ is differentiable, any minimizer of the Tikhonov functional (10) has to satisfy the first order optimality conditions

$$F'^*(c)(m^\delta - F(c)) + \alpha\mathcal{R}'(c) = 0, \qquad (11)$$

which will be the basis for the formulation of iterative algorithms for minimizing the Tikhonov functional (10). Here F'^* denotes the adjoint of the derivative operator; see also section III. For the solution of the optimality system, we consider Newton-type iterations of the form

$$\begin{aligned}\left[F'^*(c_k)F'(c_k) + \alpha_k\widetilde{\mathcal{R}}''(c_k)\right](c_{k+1} - c_k) \\ = F'^*(c_k)\left[m^\delta - F(c_k)\right] + \alpha_k\mathcal{R}'(c_k),\end{aligned} \qquad (12)$$

where $\widetilde{\mathcal{R}}''$ is an approximation for the Hessian of the regularizing functional $\mathcal{R}$. Note that by construction, any stationary point of the iteration (12) also satisfies the first order optimality conditions (11).

Since the inverse problem (9) is underdetermined, the choice of the regularization term will have significant influence on the quality of the reconstructions. As a benchmark, we will consider standard L^2-regularization, in which case

$$\mathcal{R}(c) = \tfrac{1}{2}\|c\|^2_{L^2}, \qquad \mathcal{R}'(c) = c, \qquad \mathcal{R}''(c) = I. \qquad (13)$$

From (11) and the smoothness of the adjoint operator F'^* it follows that L^2-regularization yields smooth reconstructions, which may oscillate near jumps of the solution due to the Gibbs-phenomenon. In order to be able to approximate also jumps in the solutions in a stable way, we consider a relaxed

version of total-variation regularization [17], where

$$\mathcal{R}(c) = \int_\Omega \sqrt{\beta + |\nabla c|^2} dx, \tag{14}$$
$$\mathcal{R}'(c)h = \int_\Omega \frac{\nabla c \cdot \nabla h}{\sqrt{\beta + |\nabla c|^2}} dx, \quad \langle \widetilde{R}''(c)r, h\rangle = \mathcal{R}'(c)h,$$

where $\beta > 0$ is some relaxation parameter. As a third choice, we utilize a regularization term that is related to a method of levelset-type, namely

$$\mathcal{R}(c) = \|H_\beta^{-1}(c)\|_{L^2}^2, \tag{15}$$
$$\mathcal{R}'(c) = H_\beta'(c)^{-1} H_\beta^{-1}(c), \quad \widetilde{\mathcal{R}''}(c) = H_\beta'(c)^{-2},$$

where H_β is a smooth, strictly monotonically increasing function. For the numerical tests in section IV, we use the sigmoidal function

$$H_\beta(x) = c_l + \tfrac{1}{2}\big(\mathrm{erf}(x/\beta) + 1\big)(c_u - c_l), \tag{16}$$

with relaxation parameter $\beta > 0$. Such a choice promotes bi-modal concentration distributions with lower and upper concentration niveau c_l and c_u, respectively.

For this third choice of a regularization term, the unknown fluorophore concentration can be parameterizd by a levelset function ϕ as $c = H_\beta(\phi)$, and a Newton-type iteration similar to (12), but now for the levelset function ϕ, can be used for finding a solution of (11). In fact, the inverse problem (9) can then be rephrased as $F_\beta(\phi) = M^\delta$ where $F_\beta(\phi) := F(H_\beta(\phi))$. The formulation of the corresponding Tikhonov functional, and the derivation of the optimality system and the Newton-type iteration is then straight forward; see [18] for details.

III. Numerical realization

Application of the forward operator and its derivative require the solution of systems of linear partial differential equations, e.g. (1)–(4). For an efficient discretization, we use standard finite element methods with continuous, piecewise linear finite elements [19]. The fluorophore distribution c can be expanded with respect to the same basis as the photon densities φ_i, $i = x, m$.

A. Discretized forward problems

The coordinate vectors of the finite element solutions of (1)–(4) for a set of sources $q = [q^1, \dots, q^s]$ are stored in the columns of the matrices V_x, V_m. These are obtained as solutions of the linear systems

$$[K(\kappa_x) + D(\mu_x) + B(\rho_x)]V_x = Q(q), \tag{17}$$
$$[K(\kappa_m) + D(\mu_m) + B(\rho_m)]V_m = D(\gamma c)V_x.$$

The matrices $K(\kappa_i)$, $D(\mu_i)$, $B(\rho_i)$ stem from integration of the diffusion, absorption and boundary terms with corresponding parameters, i.e. K denotes the stiffness matrix, D the mass matrix and B the boundary mass matrix. The columns of the matrix $Q(q)$ are assembled by integration of the source terms, and the measurements are finally given by $M = EV_m$, where E is a matrix mapping the solution field to the measurement data according to (6).

B. The discretized Tikhonov functional

The discrete Tikhonov functional is given by

$$J_h(c) = \tfrac{1}{2}\sum_{i,j} |M_{ij}(c) - M_{ij}^\delta|^2 + \alpha R(c), \tag{18}$$

where R is a discretization of the regularization term, and $M_{ij}(c)$ denotes the measurements corresponding to the parameter c. Note that one could easily include weighting or correlation matrices in the least squares term.

The derivative of this regularized least-squares functional in direction h then has the form

$$J_h'(c)h = Re\Big(\sum_{i,j}\Big(\overline{M_{ij}(c) - M_{ij}^\delta}\Big)\,\Delta M_{ij}(c)\Big) + \alpha R'(c)h,$$

where R' denotes the derivative of the discretized regularization term, and $\Delta M = EW_m = F'(c)h$ denotes the directional derivative of the forward map. The matrices W_m, W_x (i.e. the derivatives of the solutions V_x, V_m of the forward problem) are given as solutions of the *sensitivity system*

$$[K(\kappa_x) + D(\mu_x) + B(\rho_x)]W_x = -[K(\kappa_x'h) + D(\mu_x'h)]V_x,$$
$$[K(\kappa_m) + D(\mu_m) + B(\rho_m)]W_m$$
$$= -[K(\kappa_m'h) + D(\mu_m'h)]V_m + D(\gamma h)W_x.$$

The functions κ_i' and μ_i' denote the derivatives of the parameters defined in (4) with respect to the concentration c.

C. Adjoints and sensitivities

Let us shortly comment on the efficient assembly of the system matrix for the iteration (12). The application of the adjoint derivative $S_k^* := F'(c_k)^*$ to some element $r \in \mathbb{C}^{d\times s}$ (in the space of measurements) can be realized as follows: Let P_x, P_m denote the solutions of the adjoint system

$$[K(\kappa_m) + D(\overline{\mu_m}) + B(\rho_m)]P_m = E^T r. \tag{19}$$
$$[K(\kappa_x) + D(\overline{\mu_x}) + B(\rho_x)]P_x = D(\gamma c)]P_m.$$

Then the action of the discretized adjoint derivative S_k^* is given by $S_k^* r = \sum_{i,j}[S_k]_{ij} r_{ij}$ where the vectors $[S_k]_{ij}$, $1 \le i \le s$, $1 \le j \le d$ are defined by

$$D(1)[S_k]_{ij} = -K(\kappa_m' P_m^i)V_m^j - D(\mu_m' P_m^i)V_m^j - K(\kappa_x' P_x^i)V_x^j$$
$$- D(\mu_x' P_x^i)V_x^j + D(\gamma P_x^i)V_m^j. \tag{20}$$

Hence a matrix representation of S_k respectively S_k^* can be assembled by solving (i) the forward problem (17) with s right hand sides, (ii) the adjoint system (19) with j right hand sides, and using the representation (20).

The discretization of the regularization terms required for the iteration (12) is finally given by

$$\mathcal{R}'(c) = D(1)c, \qquad \widetilde{\mathcal{R}}''(c) = D(1)$$

in case of L^2-regualrization, and by

$$\mathcal{R}'(c) = K(c_\beta)c, \quad \widetilde{\mathcal{R}}''(c) = K(c_\beta), \quad c_\beta := \frac{1}{\sqrt{\beta + |\nabla c|^2}}$$

for the total-variation regularization. Note that by substitution $c = H_\beta(\phi)$, the regularization term (15) of the levelset-type method amounts to L^2-regularization for the levelset function ϕ and needs no further discussion.

IV. Results

Our numerical tests are performed on a cylinder with a diameter of 30 mm and a height of 60 mm. 48 optodes (24 sources and 24 detectors) are placed on 3 rings at the boundary with a spacing of 10 mm between them. A sketch of the arrangement is depicted in Fig. 1. In Table I we list the background tissue parameters for excitation and emission wavelength, which have been compiled from literature [20], [21], [22].

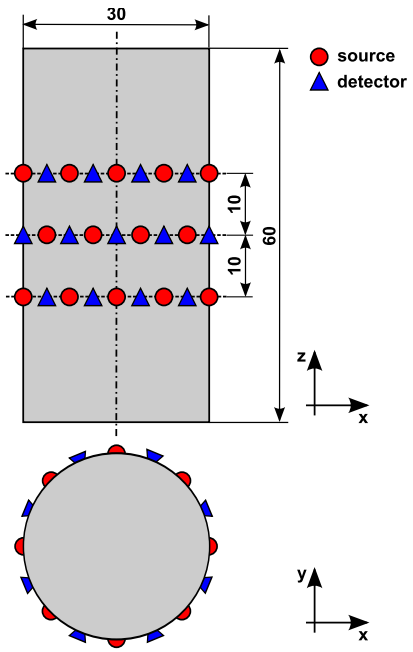

Fig. 1. For the numerical experiment a 30 mm × 60 mm cylinder model with 48 optodes on three rings spaced by 10 mm was used.

TABLE I
Values of optical parameters used for the forward simulation compiled from [20], [21], [22], [23].

	μ_s' mm^{-1}	$\mu_{a,i}$ mm^{-1}	ε $\mathrm{mm}^{-1}\,\mathrm{M}^{-1}$	ρ
excitation	0.275	0.036	$8.35 \cdot 10^3$	0.2
emission	0.235	0.029	$2.81 \cdot 10^3$	0.2

For our numerical tests, we use synthetic measurement data that are assembled by finite element simulations on a fine mesh. We incorporate tissue autofluorescence into the forward model by adding a uniformly distributed random background fluorophore concentration, cf. [24]. This results in an relative error in the measurement data of around 3 % in the ℓ^2-norm. Additionally, Gaussian noise with zero mean and a relative standard deviation of 2 % is added to the synthetic data, such that the overall relative error in the data is around 5 %.

In order to avoid inverse crimes, we use finite element methods on a coarser mesh for the reconstructions. It is assumed that all tissue properties except the concentration of the fluorphore are known beforehand; in practice, these parameters could be estimated a-priori by other imaging modalities or additional measurements.

A. Test case 1

In the first experiment, we consider a spherical fluorophore inclusion with a diameter of 5 mm at a depth of 5 mm; cf. Fig. 2(a), which displays the cross section at half height of the cylinder. For the reconstruction, we utilize Tikhonov-type methods with the three different regularization terms discussed in section II-B, and for the minimization of the Tiklhonov functionals, we employ the iteratively regularized Gauss-Newton schemes (12), where the parameter α_k is reduced successively. The algorithm is stopped when the regularization parameter reaches a predefined minimum value. For our numerical tests, the bounds have been set to $\alpha_{min} = 1 \times 10^{-4}$ for the L^2 regularization, $\alpha_{min} = 1 \times 10^{-7}$ for the TV reconstruction, and to $\alpha_{min} = 1 \times 10^{-9}$ for the method of levelset type. The relaxation parameter is set to $\beta = 1 \times 10^{-10}$ for the TV regularization and to $\beta = 1$ for the levelset type approach.

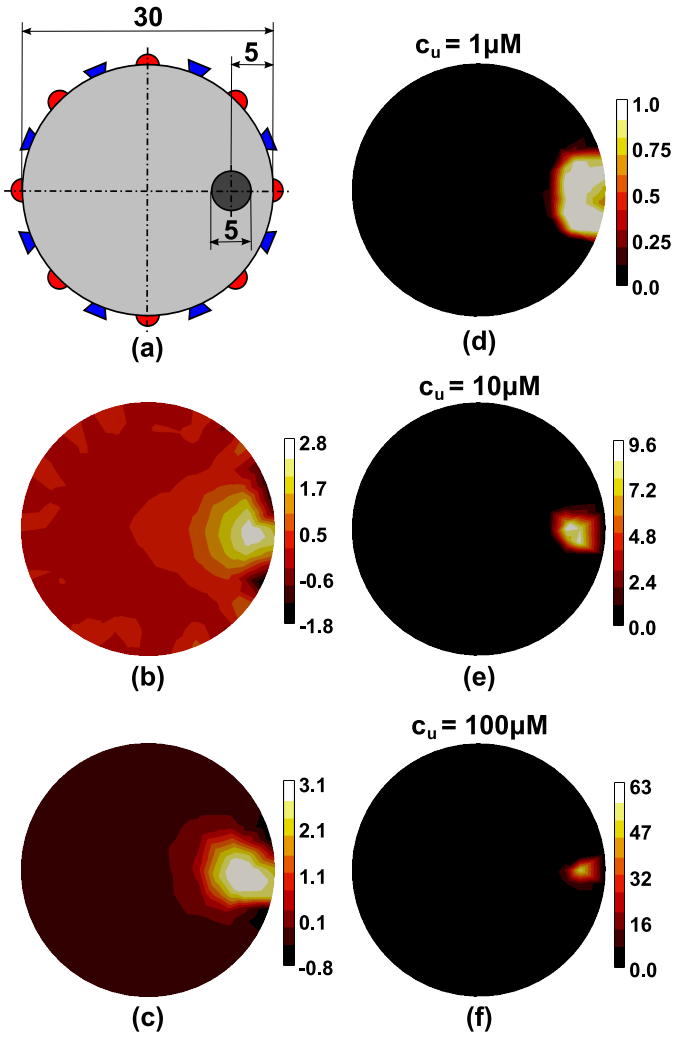

Fig. 2. Comparison of the reconstructed images of (a) a single fluorescent sphere with a concentration of 10 μM using (b) L^2 regularization, (c) TV regularization and a (d-f) levelset method with three different upper concentration niveaus c_u. Displayed are the cross sections at half height of the cylinder.

The L^2 reconstruction (Fig. 2(b)) clearly exhibits a Gibbs-phenomenon, so-called ringing artifacts, around the center

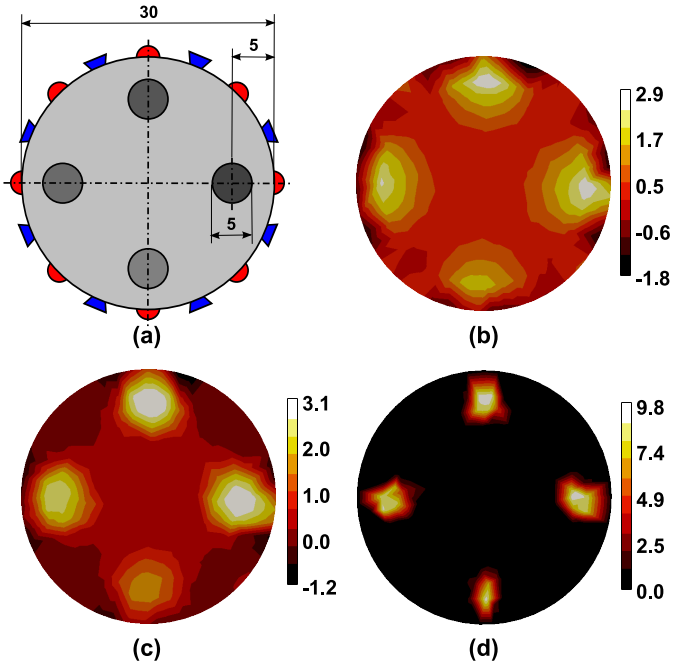

Fig. 3. (a) Simulation model including four spherical perturbations with concentrations of 10 μM, 9 μM, 8 μM and 7 μM (ccw, starting with the right one) and its reconstructions using (b) L^2 regularization, (c) TV regularization and (d) a levelset type method.

of the inclusion. The reconstructed object is also smoothed considerably making the border between the object and the background hard to distinguish. The reconstructions obtained with TV regularization (Fig. 2(c)) have a much more homogeneous background, and the transition from the object to the background is sharper. Note that both, L^2- and TV-regularization underestimate the maximal fluorophore concentration on expense of an enlarged region occupied by the fluorophore.

As the second column of Fig. 2 illustrates, the size of the inclusions reconstructed by the levelset-type method depend on the values used for upper concentration niveau c_u in (16). Since this dependence is not very strong, one can expect that reasonable approximate a-priori guesses for c_u already yield good reconstructions. Also note, that the reconstructions show a very good localization, which was the aim of introducing the nonlinear regularization terms.

B. Test case 2

In our second test case, we place four spherical fluorescent targets with a diameter of 5 mm at a distance of 5 mm from the boundary in the mid-plane of the cylinder; see Fig. 3(a). Different fluorophore concentrations of 10 μM, 9 μM, 8 μM and 7 μM are associated to the spheres in counter-clockwise direction starting with the right-most one. Fig. 3(b)-(d) displays cross section images of the reconstructions obtained with L^2-, levelset-type, and TV-regularization, respectively.

Like in the previous example, the L^2 reconstruction suffers from ringing artifacts, and is not very well localized. The TV method eliminates these artifacts, and yields better localization and slightly better quantitative estimates of the fluorophore concentrations. Note also that the relative strenghts of the different inclusions are reconstructed correctly. The best results are again obtained by the levelset-type method. Although in principle, the function H_β could be chosen to be space dependent, or also to promote several different values, we have decided to use a simple function here, which incorporates only the a-priori knowledge about the maximal expected fluorophore concentration. Due to this choice, the fluorophore concentrations at the weak inclusions are slightly overestimated on the expense of a slight underestimation of the sizes of the inclusions.

TABLE II
COMPARISON OF RECONSTRUCED FLUORESCENT INCLUSIONS.

Sphere location	Concentration (μM)				FWHM (mm)		
	original	L^2	TV	LS	L^2	TV	LS
0°	10.0	2.7	2.9	9.4	12.5	7.5	5.3
90°	9.0	2.9	3.0	9.4	10.9	6.7	4.5
180°	8.0	2.5	2.4	8.9	11.2	7.4	4.6
270°	7.0	1.8	1.5	9.5	11.0	7.8	3.8

In Fig. 4, we display profiles of the reconstructed fluorophore concentration along the x-axis. This plot highlights that the L^2- and TV-regularization substantially underestimate the concentration in the fluorophore whereas the method of levelset-type provides rather accurate reconstructions. A comparison of the maximum fluorophore concentration of the different inclusions is given in Table II.

The horizontal bars below the curves in Fig. 4 are centered at the peak concentration values and their width is equal to the full-width at half-maximum (FWHM) of the respective concentration. Along the x-axis, the smallest FWHM is obtained with the levelset method followed by the L^2-regularization and finally the TV reconstruction.

However, different half-width measures are obtained when considering the whole transversal plane instead of only the axes. The maximum FWHM-diameter of all four inclusions is to be found in Table II. The L^2 reconstruction clearly has the worst performance which is due to the large spread in the angular direction. The total-variation algorithm has fairly good agreement with the original object size. The best result is again obtained using the levelset formulation. However, this algorithm tends to slightly underestimate the object size if the upper concentration niveau is too large which can be seen from the result of the sphere with the lowest concentration (last column in Table II).

V. DISCUSSION

In this paper, we compare three different reconstruction methods for fluorescence tomography with small inclusions. The standard L^2-regularization exhibits typical ringing artifacts and smoothed reconstructions, resulting in a substantial underestimation of the maximal fluorophore concentrations. The two nonlinear regularization methods, namely total-variation regularization and the method of levelset-type, eliminate the ringing artifacts, and provide better localization of the reconstructed inclusions.

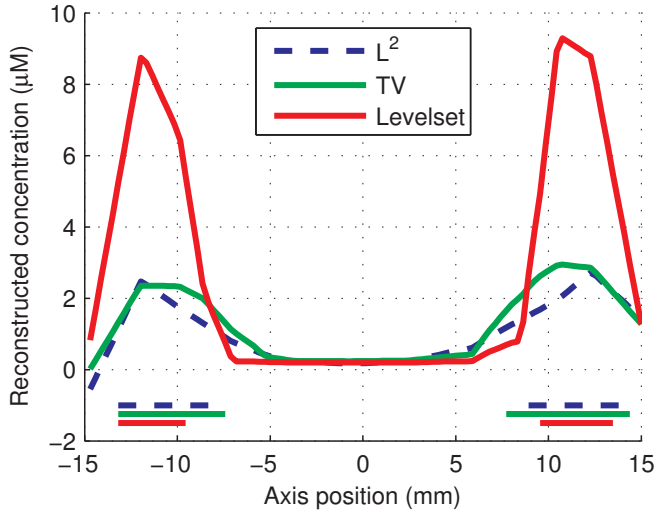

Fig. 4. Reconstructed concentrations along the x-axis of the cylinder's midplane for all three reconstruction methods. The horizontal bars below the concentration curves represent the location and full-width at half-maximum of the objects.

We would like to mention, that a different levelset approach has been investigated for fluorescence lifetime imaging in [24]. The method proposed here utilizes a relaxation of the original levelset formulation, which facilitates the reconstruction and allows to exploit algorithms very similar to L^2-regularization, which are widely used in practice, and with a comparable numerical effort.

The iterative methods used for minimizing the Tikhonov functionals utilize decaying sequences of parameters α_k. This allows to circumvent expensive line searches typically required to ensure global convergence of Newton-type iterations. This strategy also enables to choose the regularization parameter adaptively, e.g. by a discrepancy principle. For our numerical test, we chose a different strategy: we performed several reconstructions on typical known phantoms, and then determined a suitable regularization parameter, which gave good reconstructions in all cases.

As we have demonstrated by our numerical tests, the reconstructions obtained by the levelset-type method are not very sensitive to the choice of the maximal expected fluorescent dye concentrations c_u. In principle, this parameter could be estimated in the reconstruction as well.

VI. Conclusion

We have presented algorithms for fluorescence tomography using the full non-linear forward problem together with two nonlinear regularization strategies to overcome the inherent smoothness of typical fluorescence optical tomography reconstructions. The elimination of background variations enhances the contrast and facilitates the detection and separation of inclusions.

References

[1] I. S. Longmuir and J. A. Knopp, "Measurement of tissue oxygen with a fluorescent probe," *J Appl Physiol*, vol. 41, no. 4, pp. 598–602, 1976. [Online]. Available: http://jap.physiology.org/cgi/content/abstract/41/4/598

[2] E. Shives, Y. Xu, and H. Jiang, "Fluorescence lifetime tomography of turbid media based on an oxygen-sensitive dye," *Opt. Express*, vol. 10, pp. 1557–1562, 2002.

[3] S. Mordon, V. Maunoury, J. M. Devoisselle, Y. Abbas, and D. Coustaud, "Characterization of tumorous and normal tissue using a ph-sensitive fluorescence indicator (5,6-carboxyfluorescein) in vivo." *J Photochem Photobiol B*, vol. 13, no. 3-4, pp. 307–314, May 1992.

[4] I. Gannot, I. Ron, F. Hekmat, V. Chernomordik, and A. Gandjbakhche, "Functional optical detection based on ph dependent fluorescence lifetime." *Lasers Surg Med*, vol. 35, no. 5, pp. 342–348, 2004. [Online]. Available: http://dx.doi.org/10.1002/lsm.20101

[5] Y. Y. Chen and A. W. Wood, "Application of a temperature-dependent fluorescent dye (rhodamine b) to the measurement of radiofrequency radiation-induced temperature changes in biological samples," *Bioelectromagnetics*, vol. 30, pp. 583–590, 2009.

[6] G. Zacharakis, J. Ripoll, R. Weissleder, and V. Ntziachristos, "Fluorescent protein tomograpy scanner for small animal imaging," *IEEE Transactions on Medical Imaging*, vol. 24, pp. 878–885, 2005.

[7] J. S. Reynolds, T. L. Troy, and E. M. Sevick-Muraca, "Multipixel techniques for frequency-domain photon migration imaging," *Biotechnol. Prog.*, vol. 13, pp. 669–690, 1997.

[8] A. B. Milstein, S. Oh, K. J. Webb, C. A. Bouman, Q. Zhang, D. A. Boas, and R. P. Millane, "Fluorescence optical diffusion tomography," *Applied Optics*, vol. 42, pp. 3081–3094, 2003.

[9] D. S. Elson, I. Munro, J. Requejo-Isidro, J. McGinty, C. Dunsby, N. Galletly, G. W. Stamp, M. A. A. Neil, M. J. Lever, P. A. Kellett, A. Dymoke-Bradshaw, J. Hares, and P. M. W. French, "Real-time time-domain fluorescence lifetime imaging including single-shot acquisition with a segmented optical image intensifier," *New Journal of Physics*, vol. 6, p. 180, 2004. [Online]. Available: http://stacks.iop.org/1367-2630/6/180

[10] M. J. Eppstein, D. E. Dougherty, T. L. Troy, and E. M. Sevick-Muraca, "Biomedical optical tomography using dynamic parameterization and bayesian conditioning on photon migration measurements," *Applied Optics*, vol. 38, pp. 2138–2150, 1999.

[11] M. A. O'Leary, D. A. Boas, X. D. Li, B. Chance, and Y. G. Yodh, "Fluorescence lifetime imaging in turbid media," *Opt. Lett.*, vol. 21, pp. 158–160, 1996.

[12] V. Ntziachristos and R. Weissleder, "Experimental three-dimensional fluorescence reconstruction of diffuse media by use of a normalized born approximation," *Optics Letters*, vol. 26, pp. 893–895, 2001.

[13] A. Joshi, W. Bangerth, and W. M. Sevick-Muraca, "Adaptive finite element based tomography for fluorescence optical imaging in tissue," *Opt. Express*, vol. 12, pp. 5402–5417, 2004.

[14] E. M. Sevick-Muraca, E. Kuwana, A. Godavarty, J. P. Houston, A. B. Thompson, and R. Roy, "Near-infrared fluorescence imaging and spectroscopy in random media and tissue," in *Biomedical Photonics Handbook*, T. Vo-Dinh, Ed. Boca Raton: CRC Press, 2003, ch. 33.

[15] T. J. Farell and M. S. Patterson, "Diffusion modeling of fluorescence in tissue," in *Handbook of Biomedical Fluorescence*, M.-A. Mycek and B. W. Pogue, Eds. New York, Basel: Marcel Dekker Inc., 2003, ch. 2.

[16] S. R. Arridge, "Optical tomography in medical imaging," *Inverse Problems*, vol. 15, pp. R41–R93, 1999.

[17] R. Acar and C. R. Vogel, "Analysis of bounded variation penalty methods for ill-posed problems," *Inverse Problems*, vol. 10, pp. 1217–1229, 1994.

[18] H. Egger and A. Leitao, "Nonlinear regularization methods for ill-posed problems with piecewise constant or strongly varying solutions," *Inverse Problems*, vol. 25, p. 115014, 2009.

[19] P. Ciarlet, *The finite element method for elliptic problems*. Amsterdam, New York: North-Holland, 1978.

[20] G. Alexandrakis, F. R. Rannou, and A. F. Chatziioannou, "Tomographic bioluminescence imaging by use of a combined optical-pet (opet) system: a computer simulation feasibility study," *Physics in Medicine and Biology*, vol. 50, pp. 4225–4241, 2005.

[21] M. Keijzer, W. M. Star, and P. R. M. Storchi, "Optical diffusion in layered media," *Applied Optics*, vol. 27, pp. 1820–1824, 1988.

[22] A. Joshi, "Adaptive finite element methods for fluorescence enhanced optical tomography," Ph.D. dissertation, Texas A&M University, 2005.

[23] M. L. Landsman, G. Kwant, G. A. Mook, and W. G. Zijlstra, "Light-absorbing properties, stability, and spectral stabilization of indocyanine green," *J Appl Physiol*, vol. 40, no. 4, pp. 575–583, 1976. [Online]. Available: http://jap.physiology.org/cgi/content/abstract/40/4/575

[24] D. Alvarez, P. Medina, and M. Moscoso, "Fluorescence lifetime imaging from time resolved measurements using a shape-based approach," *Optics Express*, vol. 17, pp. 8843–8855, 2009.